Obliquely propagating waves in the magnetized strongly coupled one-component plasma

Hanno Kählert, Torben Ott, Alexi Reynolds, Gabor J. Kalman, and Michael Bonitz

Citation: Phys. Plasmas **20**, 057301 (2013); doi: 10.1063/1.4801522
View online: http://dx.doi.org/10.1063/1.4801522
View Table of Contents: http://pop.aip.org/resource/1/PHPAEN/v20/i5
Published by the American Institute of Physics.

Obliquely propagating waves in the magnetized strongly coupled one-component plasma[a)]

Hanno Kählert,[1,b)] Torben Ott,[2] Alexi Reynolds,[3] Gabor J. Kalman,[1] and Michael Bonitz[2]
[1]*Department of Physics, Boston College, 140 Commonwealth Ave, Chestnut Hill, Massachusetts 02467, USA*
[2]*Institut für Theoretische Physik und Astrophysik, Christian-Albrechts Universität zu Kiel, Leibnizstr. 15, 24098 Kiel, Germany*
[3]*School of Physics and Astronomy, University of Birmingham, Edgbaston, Birmingham B15 2TT, United Kingdom*

(Received 1 December 2012; accepted 4 January 2013; published online 16 April 2013)

The quasi-localized charge approximation is used to calculate the wave spectrum of the magnetized three-dimensional strongly coupled one-component plasma at arbitrary angles θ between the wave vector and the magnetic field axis. Three frequency branches are identified whose interplay is strongly determined by $\beta = \omega_c/\omega_p$, the ratio of the cyclotron frequency ω_c, and the plasma frequency ω_p. The frequency dispersion relations for the three principal modes along the magnetic field cross in the case $\beta < 1$, which strongly affects the transition from parallel to perpendicular wave propagation. For $\beta > 1$, the frequencies of the different branches are well separated, and the long-wavelength dispersion in the intermediate and upper branch changes sign as θ is varied from 0 to $\pi/2$. In addition to the frequencies, we also investigate the waves' polarization properties.
 [http://dx.doi.org/10.1063/1.4801522]

I. INTRODUCTION

Recently, there has been a growing interest in the properties of complex plasmas[1–3] in strong external magnetic fields. The available field strengths of a few Tesla are sufficient to magnetize the *weakly* coupled electrons and ions, leading to considerably modified plasma behavior. Strong magnetic fields have been shown to alter the discharge conditions[4] as well as the effective dust-dust interaction in the presence of streaming ions.[5]

Here, we are concerned with *strongly* coupled plasmas, e.g., the dust component in a complex plasma. They are characterized by a Coulomb coupling parameter

$$\Gamma = \frac{Q^2}{4\pi\epsilon_0 a}\frac{1}{k_B T} > 1, \tag{1}$$

where Q denotes the particles' charge, T is the temperature, and $a = (3/4\pi n)^{1/3}$ is the Wigner-Seitz radius (density n). In the limit $1 \ll \Gamma < \Gamma_m$, where Γ_m is the coupling parameter at which a phase transition towards a crystal occurs,[6] the plasma behavior is dominated by the so-called caging effect.[7] The strong interactions create local potential minima that trap particles for a sufficiently long time such that they can perform several small-amplitude oscillations within their local caging environment.

If an external magnetic field $\boldsymbol{B} = B\hat{e}_z$ is applied, the constituents of the plasma are affected by the Lorentz force. In order to observe magnetization effects in the strongly correlated plasmas discussed above,[8,9] it is necessary to increase

$$\beta = \frac{|\omega_c|}{\omega_p} = |B|\sqrt{\frac{\epsilon_0}{m\,n}}, \tag{2}$$

the ratio of the cyclotron frequency $\omega_c = QB/m$ and the plasma frequency $\omega_p = (Q^2 n/\epsilon_0 m)^{1/2}$ (particle mass m), to values $\beta \gtrsim 0.5$. Systems with strong magnetization include cold ions in Penning traps[10] and the plasmas in the envelopes of neutron stars.[11] On the other hand, considering the high mass of micron-sized dust particles, strong magnetization is very difficult to achieve in a complex plasma unless smaller (i.e., lighter) particles in the nm size range are used. An alternative approach, where the effect of the Lorentz force is replaced by the Coriolis force in a rotating reference frame, has recently been used to study the normal modes of a small dusty plasma crystal.[12] A rotating neutral gas column serves as a reservoir of angular momentum that is transferred to the dust particles via the neutral drag force.[13] While it may become more challenging to "magnetize" extended dust layers,[14] the dust particles experience effective magnetic fields that are orders of magnitude larger than those of superconducting magnets.

A strong magnetic field can significantly alter the dynamics of a strongly coupled plasma, e.g., its collective modes. The wave spectra of solid[15–17] and liquid[8,17–19] two-dimensional Yukawa plasmas in magnetic fields have been investigated theoretically with both simulations and (semi) analytical approaches. Other studies addressed the closely related two-dimensional one-component plasma (OCP).[20,21] It was found that the Lorentz force couples the longitudinal and the transverse waves and gives rise to the so-called upper and lower hybrid modes. In the three-dimensional (Yukawa) OCP, the strong directional dependence of the Lorentz force leads to profound differences in the diffusion properties[9] parallel and perpendicular to the field axis, depending on the coupling strength. Even though the motion along the field is not directly influenced, the parallel diffusion coefficient closely approaches the perpendicular diffusion coefficient in the strong coupling limit. The properties of lattice[22–25] or plasma[26,27] waves are also very sensitive to a magnetic field.

[a)]Paper GI3 4, Bull. Am. Phys. Soc. **57**, 110 (2012).
[b)]Invited speaker.

Electromagnetic modes in a magnetized strongly coupled plasma have been studied as well.[28] Genga studied the wave dispersion in the long-wavelength limit based on the Singwi-Tosi-Land-Sjölander theory[41] and high-frequency sum-rules.[42] Here, we work in the electrostatic limit and neglect retardation effects. They become important at very small wavenumbers, $k < \omega_p/c$,[29] see below.

In the following, we extend our previous studies of collective modes in the strongly coupled magnetized three-dimensional OCP[26,27] and concentrate on the transition from perpendicular to parallel wave propagation. In particular, we investigate how the principal modes connect as the angle between the magnetic field and the wave vector is varied. We use the quasi-localized charge approximation (QLCA),[30] which has been successfully applied to a variety of strongly correlated systems.[31] Its theoretical foundation rests on the aforementioned caging effect. As a fundamental model system, the OCP can serve as a reference to study the combined effects of strong coupling and magnetization. Thus, besides being of theoretical interest, our results for the magnetized OCP are relevant for a variety of systems including ions in Penning traps,[10] the Coulomb liquids and solids in the envelope of neutron stars,[11] rotating dusty plasmas, or magnetized "nano-dust." In particular, the collective modes directly determine their linear response behavior.

This paper is organized as follows. The QLCA theory and the principal modes of the magnetized OCP for wave propagation along and across the magnetic field are reviewed in Sec. II. The transition between these two special cases is investigated in detail in Sec. III. We focus on the frequencies and the polarization properties. We conclude with a brief summary in Sec. IV.

II. REVIEW OF QLCA AND PRINCIPAL MODES

A. QLCA for the OCP in a magnetic field

In the QLCA,[31] the collective modes of a strongly coupled plasma subject to a magnetic field $\boldsymbol{B} = B\hat{\boldsymbol{e}}_z$ are the non-trivial solutions to[27]

$$\left[\omega^2\delta_{\alpha\beta} + i\omega\omega_c\sigma_{\alpha\beta} - D_{\alpha\beta}(\boldsymbol{k}) - \frac{k_\alpha k_\beta}{k^2}\omega_p^2\right] q_{\boldsymbol{k},\beta}(\omega) = 0, \quad (3)$$

where $q_{\boldsymbol{k},\beta}$ is the particle displacement, $\sigma_{yx} = -\sigma_{xy} = 1$ and $\sigma_{\alpha\beta} = 0$ otherwise.

The dynamical matrix of the QLCA[31] can be written as

$$D_{\alpha\beta}(\boldsymbol{k}) = \left(\delta_{\alpha\beta} - \frac{k_\alpha k_\beta}{k^2}\right) D_T(k) + \frac{k_\alpha k_\beta}{k^2} D_L(k), \quad (4)$$

where $D_L(k)$ and $D_T(k)$ denote its longitudinal and transverse components, respectively. They account for the correlation corrections to the dispersion relation and are functions of the equilibrium pair correlation function $h(r)$. In the 3D OCP, they are given by[29]

$$D_T(k) = \omega_p^2 \int_0^\infty dr \frac{h(r)}{r}\left[\frac{\sin(kr)}{kr} + 3\frac{\cos(kr)}{(kr)^2} - 3\frac{\sin(kr)}{(kr)^3}\right], \quad (5)$$

and $D_L(k) = -2D_T(k)$. The pair correlation function is obtained from MD simulations.

If we choose the wave vector in the xz–plane, we have $\boldsymbol{k} = k(\sin\theta, 0, \cos\theta)$ with θ denoting the angle between the magnetic field and $\boldsymbol{k}$. It is convenient to express the displacement vector in a local basis according to

$$\boldsymbol{q_k} = q_k\hat{\boldsymbol{e}}_k + iq_\phi\hat{\boldsymbol{e}}_\phi + q_\theta\hat{\boldsymbol{e}}_\theta = \underbrace{\begin{pmatrix} \sin\theta & 0 & \cos\theta \\ 0 & i & 0 \\ \cos\theta & 0 & -\sin\theta \end{pmatrix}}_{=\boldsymbol{U}(\theta)} \begin{pmatrix} q_k \\ q_\phi \\ q_\theta \end{pmatrix}, \quad (6)$$

where $\hat{\boldsymbol{e}}_k, \hat{\boldsymbol{e}}_\phi$, and $\hat{\boldsymbol{e}}_\theta$ are the usual unit vectors in spherical coordinates in the xz-plane ($\phi = 0$).

Multiplying Eq. (3) from the left by $\boldsymbol{U}^\dagger(\theta)$ and using Eq. (6), we obtain

$$\begin{pmatrix} \omega^2 - \omega_P^2(k) & \omega\omega_c\sin\theta & 0 \\ \omega\omega_c\sin\theta & \omega^2 - \omega_{OS}^2(k) & \omega\omega_c\cos\theta \\ 0 & \omega\omega_c\cos\theta & \omega^2 - \omega_{OS}^2(k) \end{pmatrix} \begin{pmatrix} q_k \\ q_\phi \\ q_\theta \end{pmatrix} = 0, \quad (7)$$

where the frequencies of the plasmon (P) and the ordinary shear (OS) mode are given by

$$\omega_P(k) = \sqrt{\omega_p^2 + D_L(k)}, \quad (8)$$

$$\omega_{OS}(k) = \sqrt{D_T(k)}, \quad (9)$$

respectively. They correspond to the principal modes of the QLCA in the unmagnetized OCP.[29] The eigenfrequencies in the magnetized system are the roots of

$$\omega^2\omega_c^2\{[\omega^2 - \omega_P^2(k)]\cos^2\theta + [\omega^2 - \omega_{OS}^2(k)]\sin^2\theta\} = [\omega^2 - \omega_P^2(k)][\omega^2 - \omega_{OS}^2(k)]^2. \quad (10)$$

The wave properties, i.e., their longitudinal and transverse components and polarizations, are determined by the components of the displacement vector $\boldsymbol{q_k}$. It leads to the following particle motion

$$\begin{aligned} \boldsymbol{q}(\boldsymbol{r}, t) &\sim \Re[\boldsymbol{q_k}(\omega)\, e^{i(\boldsymbol{k}\cdot\boldsymbol{r} - \omega t)}] \\ &= q_k\,\hat{\boldsymbol{e}}_k\cos(\boldsymbol{k}\cdot\boldsymbol{r} - \omega t) \\ &\quad - q_\phi\,\hat{\boldsymbol{e}}_\phi\sin(\boldsymbol{k}\cdot\boldsymbol{r} - \omega t) + q_\theta\,\hat{\boldsymbol{e}}_\theta\cos(\boldsymbol{k}\cdot\boldsymbol{r} - \omega t), \end{aligned} \quad (11)$$

where q_k, q_ϕ, and q_θ are real numbers with $q_k^2 + q_\theta^2 + q_\phi^2 = 1$.

The magnitude of the longitudinal component is determined by $|q_k|$, i.e., $|q_k| = 1$ for a purely longitudinal wave and $|q_k| = 0$ for a transverse wave. The remaining elliptical motion in the $\phi - \theta$ plane can be characterized by the modified eccentricity[27]

$$\epsilon = \gamma\sqrt{1 - \frac{b^2}{a^2}}, \quad (12)$$

where $a = \max(|q_\phi|, |q_\theta|), b = \min(|q_\phi|, |q_\theta|)$, and $\gamma = 1$ if $|q_\theta| > |q_\phi|$ and -1 otherwise. We get $\epsilon = 1$ for a wave that

is linearly polarized along $\hat{\boldsymbol{e}}_\theta, \epsilon = -1$ for linear polarization along $\hat{\boldsymbol{e}}_\phi$, and $\epsilon = 0$ for circular polarization. Note that the definition of ϵ is based on different axes than in Ref. 27.

B. Principal waves: $\boldsymbol{k} \parallel \boldsymbol{B}$ and $\boldsymbol{k} \perp \boldsymbol{B}$

The three modes for $\theta = 0$ are the plasmon [Eq. (8)] and the upper shear (US) and lower shear (LS) modes with[27]

$$\omega_{\mathrm{US,LS}}(k) = \frac{1}{2}\left[\sqrt{\omega_\mathrm{c}^2 + 4\omega_\mathrm{OS}^2(k)} \pm |\omega_\mathrm{c}|\right]. \tag{13}$$

While the plasmon is a longitudinal mode ($|q_k| = 1$) and unaffected by the Lorentz force, the upper and lower shear modes are transverse excitations ($|q_k| = 0$). They originate from the two degenerate shear modes in the unmagnetized limit and are circularly polarized ($\epsilon = 0$). Their frequencies are separated by the cyclotron frequency.

For wave vectors at an angle $\theta = \pi/2$ with respect to $\boldsymbol{B}$, the excitation spectrum consists of the ordinary shear mode [Eq. (9)] and the upper (UH) and lower (LH) hybrid modes[27]

$$\omega_{\mathrm{UH,LH}}^2(k) = \frac{1}{2}[\omega_\mathrm{c}^2 + \omega_\mathrm{P}^2(k) + \omega_\mathrm{OS}^2(k) \pm \sqrt{[\omega_\mathrm{P}^2(k) - \omega_\mathrm{OS}^2(k) + \omega_\mathrm{c}^2]^2 + 4\omega_\mathrm{c}^2\omega_\mathrm{OS}^2(k)}]. \tag{14}$$

The OS mode is acoustic with[29,32]

$$\lim_{k\to 0}\frac{\omega_\mathrm{OS}(k)}{k} = c_\mathrm{OS}(\Gamma) = \sqrt{\alpha(\Gamma)}\,\omega_\mathrm{p}\,a, \tag{15}$$

where $c_\mathrm{OS}(\Gamma)$ is the associated acoustic speed, $\alpha(\Gamma) = -\frac{2}{45}\frac{\mathcal{E}_\mathrm{c}(\Gamma)/\Gamma}{k_\mathrm{B}T}$, and $\mathcal{E}_\mathrm{c}(\Gamma)$ the (negative) correlation energy per particle of the OCP.[33] The QLCA yields the acoustic speed of the LH mode as

$$c_\mathrm{LH}(\Gamma,\beta) = \frac{c_\mathrm{OS}(\Gamma)}{(1+\beta^2)^{1/2}}. \tag{16}$$

One must keep in mind, however, that it does not include the diffusive motion of the particles and the associated slow change of the potential landscape, which causes the damping of the shear mode in a real liquid at long wavelengths and low frequencies.[31,34,35] Indeed, our simulations have shown that the OS, LS, and LH modes exist only beyond a critical wave vector.[27]

Just like the plasmon at $\theta = 0$, the OS mode is independent of the magnetic field. It is linearly polarized ($|q_k| = 0, \epsilon = 1$) with particle displacements along $\boldsymbol{B}$. The upper and lower hybrid modes, on the other hand, exhibit elliptical polarizations ($\epsilon = -1, |q_k| \geq 0$), where the particle displacements are within the xy–plane, see Ref. 27 for more details.

III. WAVE PROPAGATION AT OBLIQUE ANGLES

We now extend the discussion of the excitation spectrum to arbitrary directions of the wave vector.

A. Wave dispersion

It is possible to make some general statements about the eigenfrequencies $\{\omega_i\}$. Just like the frequencies of a crystalline lattice,[22,24] they satisfy a generalized Kohn sum rule in a magnetic field

$$\sum_{i=1}^{3}\omega_i^2(\boldsymbol{k}) = \omega_\mathrm{p}^2 + \omega_\mathrm{c}^2. \tag{17}$$

Likewise,[36] one can derive the fourth-order frequency sum

$$\sum_{i=1}^{3}\omega_i^4(\boldsymbol{k}) = \omega_\mathrm{P}^4(k) + 2\omega_\mathrm{OS}^4(k) + \omega_\mathrm{c}^2\{\omega_\mathrm{c}^2 + \omega_\mathrm{p}^2 + \omega_\mathrm{OS}^2(k) + [\omega_\mathrm{OS}^2(k) - \omega_\mathrm{P}^2(k)]\cos(2\theta)\}, \tag{18}$$

which is explicitly $\boldsymbol{k}$-dependent.

1. Long- and short-wavelength limit

In the long-wavelength limit, $k \to 0$, the longitudinal and transverse components of the dynamical matrix vanish, i.e., $\omega_\mathrm{P}(k) \to \omega_\mathrm{p}, \omega_\mathrm{OS}(k) \to 0$. This implies that the frequencies in this limit are determined by the mean-field contribution only. Thus, we obtain $\omega_1^0 = 0$ and the gap frequencies

$$\omega_{2,3}^0 = \sqrt{\frac{1}{2}[\omega_\mathrm{c}^2 + \omega_\mathrm{p}^2 \mp \sqrt{\omega_\mathrm{c}^4 + \omega_\mathrm{p}^4 - 2\omega_\mathrm{c}^2\omega_\mathrm{p}^2\cos(2\theta)}]}, \tag{19}$$

with $\omega_1^0 \leq \omega_2^0 \leq \omega_3^0$, see also Ref. 37 for a cold ideal plasma and Ref. 24 for the OCP crystal.

Note that strictly speaking for very long wavelengths, $k < \omega_\mathrm{p}/c$, the electromagnetic term in the dispersion relation must be restored, which ensures that the dispersion at $k \equiv 0$ is isotropic. The frequencies that are characterized by $(kc/\omega)^2 = 0$ are usually known as the cutoff frequencies. In a cold ideal plasma, the gap frequencies $\omega_{2,3}^0$ [Eq. (19)], on the other hand, correspond to the regime where $(kc/\omega)^2 \to \infty$ and are referred to as resonances.[28,37,38] Their angular dependence is depicted in Fig. 1, together with the angle-independent cutoff frequency[37] $\omega_\mathrm{co} = \frac{1}{2}\left[\sqrt{\omega_\mathrm{c}^2 + 4\omega_\mathrm{p}^2} - |\omega_\mathrm{c}|\right]$, which is relevant for the modes here. A deeper analysis of the wavenumber domain $k < \omega_\mathrm{p}/c \ll a^{-1}$ is, however, beyond the scope of this paper, see Refs. 28, 37, and 38 for details.

The small k expansions of the frequencies are affected by correlations. Using the expansion of the OS mode [Eq. (15)] and $\omega_\mathrm{P}(k) \approx \omega_\mathrm{p}[1 - \alpha(\Gamma)\,k^2a^2]$,[29] we find from Eq. (10)

$$\omega_1(k,\theta) \approx \frac{\omega_\mathrm{p}}{|\cos\theta|}\frac{\alpha(\Gamma)}{\beta}k^2a^2, \tag{20}$$

$$\omega_{2,3}(k,\theta) \approx \omega_{2,3}^0(\theta) \times\left[1 \pm \frac{\alpha(\Gamma)}{4}\frac{4 - \beta^2[1+3\cos(2\theta)]}{\sqrt{1+\beta^4-2\beta^2\cos(2\theta)}}\frac{\omega_\mathrm{p}^2}{(\omega_{2,3}^0)^2}k^2a^2\right]. \tag{21}$$

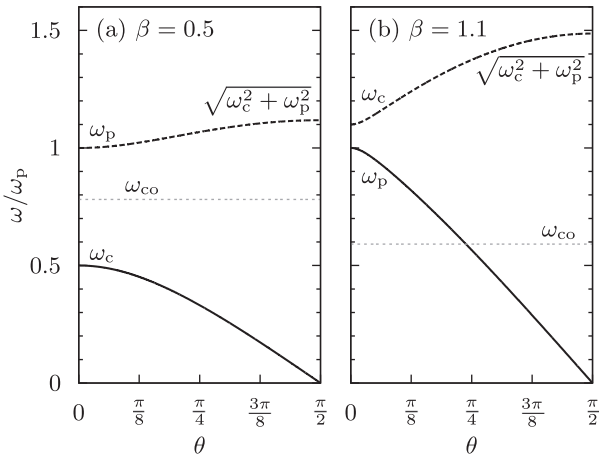

FIG. 1. Dependence of the gap frequencies ω_2^0 (solid lines) and ω_3^0 (dashed lines) on θ [Eq. (19)] for (a) $\beta < 1$ and (b) $\beta > 1$, see also Ref. 37. Their limits for $\theta \to 0$ and $\theta \to \pi/2$ are indicated in the figure. The cutoff frequency ω_{co} (see text) is shown by the horizontal lines.

Compared to strictly perpendicular wave propagation ($\theta \equiv \pi/2$), the long-wavelength dispersion of the modes in the lower and intermediate branch is quadratic for $\theta \neq \pi/2$, which was also observed in the OCP crystal.[24] The quadratic dispersion is reminiscent of a Whistler mode. A more detailed analysis of the limit $\theta \to \pi/2$ is presented in the Appendix. Equation (21) further shows that for $\beta > 1$, the dispersion of the modes in the intermediate and upper branch changes sign at the critical angle

$$\theta_{\text{crit}}(\beta) = \frac{1}{2}\arccos\left(\frac{4-\beta^2}{3\beta^2}\right) \xrightarrow[\beta\to\infty]{} 0.955(\approx 54.7^\circ). \quad (22)$$

While the $k \to 0$ frequencies are angle-dependent, the corresponding frequencies in the limit $k \to \infty$ are not. Here, the common frequency limit of the OS and P mode is the OCP Einstein frequency[29,32] $\omega_E = \omega_p/\sqrt{3}$. The magnetic field dependent asymptotes thus become[27]

$$\omega_{1,3}^{\infty} = \frac{1}{2}\left[\sqrt{\omega_c^2 + 4\omega_E^2} \mp |\omega_c|\right], \quad \omega_2^{\infty} = \omega_E. \quad (23)$$

They correspond to oscillations of a particle in a magnetized harmonic trap with isotropic confinement. The frequencies $\omega_{1,2,3}^{\infty}$ correspond to the three different polarizations of the oscillations, see Sec. III B 1.

2. Finite wave vectors

The coupling parameter mainly determines the oscillatory behavior of the dispersion curves. We chose a representative example with $\Gamma = 100$ to discuss their general features at finite wave vectors and arbitrary angles. The results are displayed in Fig. 2.

One readily observes that for certain values of k, where $\omega_P(k) = \omega_{OS}(k) = \omega_E$,[29] the frequencies become independent of the angle θ. The frequencies that follow from Eq. (10) under this constraint are identical to those in the limit $k \to \infty$, see Eq. (23).

In the high-field limit [Fig. 2(c)], the dispersion curves show the least complex behavior, and all modes are clearly separated. At high frequencies, $\omega > \omega_p$, we find a set of modes whose frequencies are bounded by those of the US and UH mode. Similar behavior is observed for the plasmon and the OS mode at intermediate, and the LH and LS modes at low frequencies. These three branches will be referred to as the high, intermediate, and low frequency branch. Their

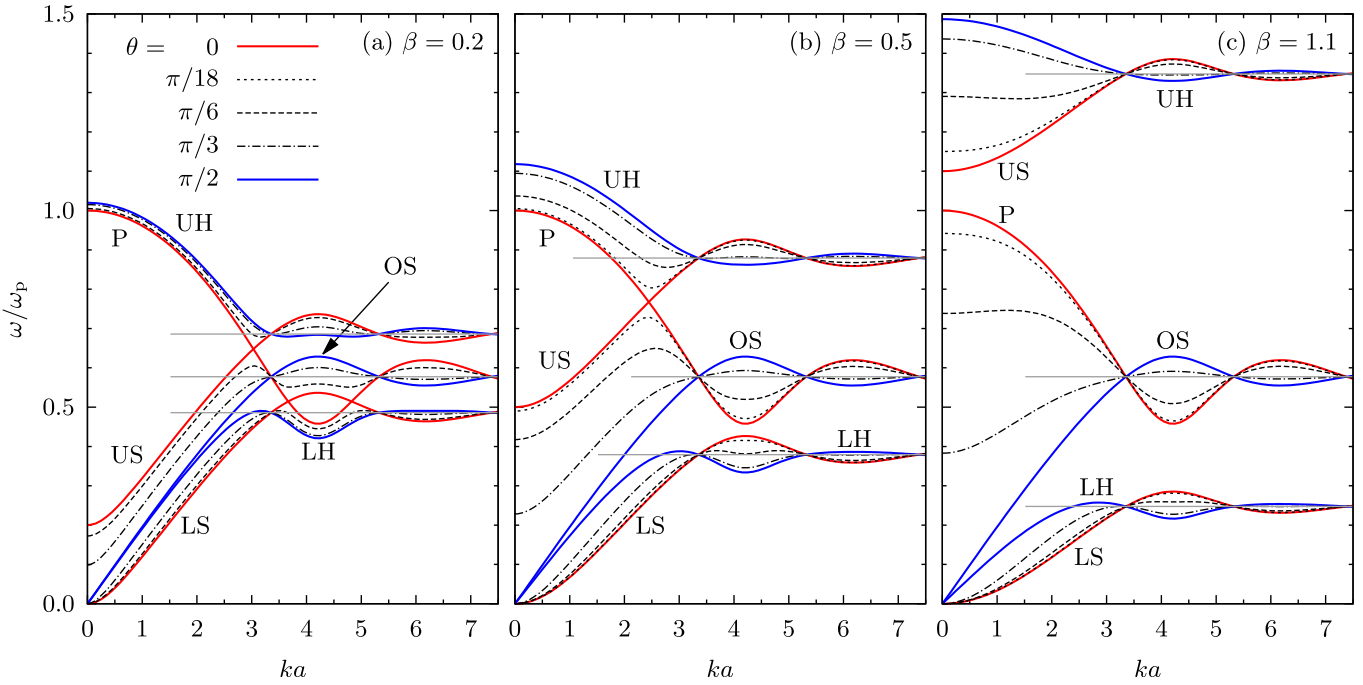

FIG. 2. Dispersion relation $\omega(k)$ at a coupling parameter $\Gamma = 100$ for (a) weak, (b) intermediate, and (c) strong magnetic fields and various angles $\theta = \angle(\boldsymbol{k}, \boldsymbol{B})$. Note that the case $\theta = \pi/18$ is not shown in panel (a). The horizontal lines show the frequency limits for $k \to \infty$, Eq. (23).

$k \to 0$ and $k \to \infty$ limiting frequencies are given by Eqs. (19) and (23), respectively.

The situation becomes more complex as we decrease the magnetic field strength [Fig. 2(b)], where the US and plasmon dispersion curves cross at $k_{\mathrm{crit}}a \approx 2.4$. This leads to an avoided crossing of the modes in the upper and intermediate branch as $\theta \to 0$. At small wavenumbers, they are now bounded from below (above) by ω_{P} (ω_{US}). The qualitative behavior of the lower branch remains unaffected.

This is changed, however, in weak magnetic fields [Fig. 2(a)], where the LS and plasmon frequencies cross. This has two consequences. First, the frequencies of the modes in the lower branch are now bounded by those of the LH mode and the minimum of ω_{P} and ω_{LS}. Second, the new lower bound of the intermediate branch in the small wavenumber interval where $\omega_{\mathrm{LS}} > \omega_{\mathrm{P}}$ is the LS frequency.

B. Wave properties

We now consider the wave properties, which are calculated from Eq. (7) using the previously obtained eigenfrequencies.

1. Long- and short-wavelength limit

With $\omega_1^0 = 0$, one can see from Eq. (7) that $|q_{k;1}^0| = 0$, i.e., the wave in the lower branch is purely transverse at $k = 0$. For $\theta \neq \pi/2$, we further obtain $\epsilon_1(k) \to 0$ as $k \to 0$, which corresponds to circular polarization. The exception is the LH mode, which has $\epsilon_1^0 = -1$ for $\theta = \pi/2$.

For the intermediate and upper branch, one finds

$$\epsilon_2^0(\theta,\beta) = \left[1 - \frac{1+\beta^2 - \sqrt{1+\beta^4 - 2\beta^2\cos(2\theta)}}{2\beta^2\cos^2\theta}\right]^{1/2},$$
$$\epsilon_3^0(\theta,\beta) = -\frac{1}{\sqrt{2}}[1-\beta^2 + \sqrt{1+\beta^4 - 2\beta^2\cos(2\theta)}]^{1/2}. \tag{24}$$

Note that for $\beta > 1$ ($\beta < 1$), the $\theta \equiv 0$ limit of the intermediate (upper) branch is the plasmon for which ϵ is not defined. The above expressions then only apply to angles $0 < \theta < \pi/2$. Further, we have $\epsilon_2^0(\theta \equiv \pi/2, \beta) = 1$ for the OS mode. The expressions for the longitudinal components are rather cumbersome. We therefore show the numerical results in Fig. 3 only, together with the eccentricities [Eq. (24)].

For $\beta < 1$, the intermediate mode is purely transverse at $\theta = 0$ (US mode), becomes partially longitudinal for $\theta > 0$, and transforms into the transverse OS mode at $\theta = \pi/2$, see Fig. 3(a). In the case $\beta > 1$, the plasmon is the mode with the second highest frequency at $\theta = 0$. Thus, the intermediate mode is purely longitudinal instead. The behavior for the high-frequency mode is very similar [Fig. 3(b)], but the roles of the P and US modes are exchanged. The $\theta \to \pi/2$ limit is now the UH mode, which has both longitudinal and transverse components, depending on the value of β.

Figures 3(c) and 3(d) show that the elliptical motion in the ϕ–θ plane is stretched along $\hat{\boldsymbol{e}}_\theta$ ($\hat{\boldsymbol{e}}_\phi$) for the modes in the intermediate (upper) branch. As noted before, some of the limiting cases require particular attention. This will be discussed in more detail in Sec. III B 2.

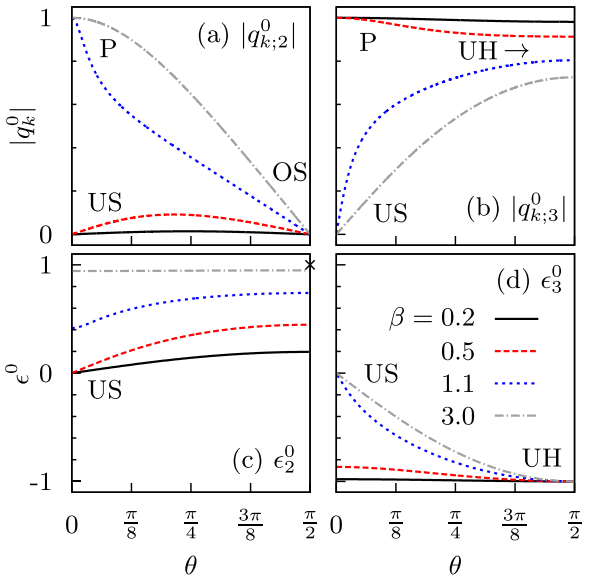

FIG. 3. Longitudinal component of the particle displacement, $|q_k|$, and modified eccentricity, ϵ, in the limit $k \to 0$ as a function of θ and various magnetic field strengths. (a), (c): intermediate branch; (b), (d): upper branch. The cross in (c) indicates the value for the OS mode at $\theta = \pi/2$.

The eigenvector for the intermediate frequency branch in the limit $k \to \infty$ is strictly along the magnetic field, which is why the Lorentz force has no effect on the wave's properties and its frequency. We get

$$|q_{k;2}^\infty| = |\cos\theta|, \quad \epsilon_2^\infty = 1 (0 < \theta \leq \pi/2), \tag{25}$$

i.e., the wave transforms from a purely longitudinal wave at $\theta = 0$ (the plasmon) into a purely transverse mode polarized along $\hat{\boldsymbol{e}}_\theta = \hat{\boldsymbol{e}}_z$ at $\theta = \pi/2$ (the OS mode). For any oblique angle, it has both a longitudinal and a transverse component with linear polarization.

For short-wavelength excitations ($k \to \infty$) in the upper and lower branch, the eigenvector describes a circular motion around the magnetic field axis. We get

$$|q_{k;1,3}^\infty| = \frac{|\sin\theta|}{\sqrt{2}}, \quad \epsilon_{1,3}^\infty = -\sin\theta, \tag{26}$$

which corresponds to the cyclotron motion of a particle in a magnetic field and an isotropic confinement (see Sec. III A 1). The motion in the upper branch is in agreement with the usual cyclotron motion, while the trajectory in the lower branch is in the opposite direction, giving rise to the lower of the two frequencies. At $\theta = 0$, the two modes correspond to the upper and lower shear modes, which are purely transverse and circularly polarized. The waves then pick up a longitudinal component for $\theta > 0$. For $\theta = \pi/2$, the $\hat{\boldsymbol{e}}_\theta$ component vanishes, and the waves transform into the upper and lower hybrid modes. The associated particle displacements are within the xy-plane, see also Ref. 27.

2. Finite wave vectors

The full wave vector dependence of $|q_k|$ and ϵ is displayed in Figs. 4 and 5. Consider first the high-field limit, Fig. 4. Just like the mode frequencies are bounded by the frequencies of the modes in the limits $\theta = 0$ and $\theta = \pi/2$, the

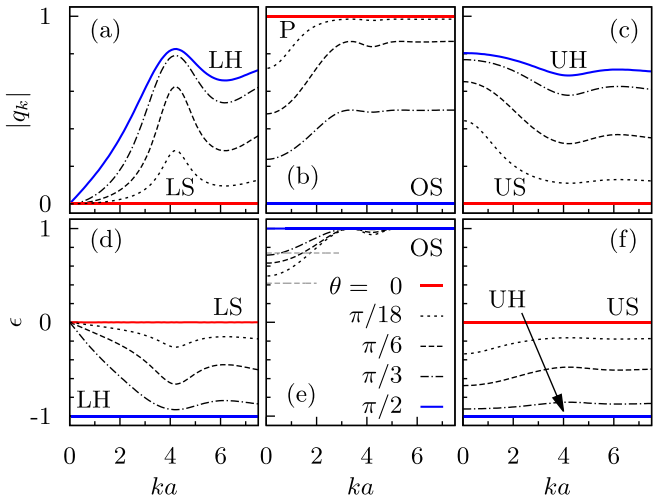

FIG. 4. Longitudinal component of the particle displacement, $|q_k|$, and modified eccentricity, ϵ, as a function of k and various angles for the same parameters as in Fig. 2(c) [$\Gamma = 100, \beta = 1.1$]—(a), (d): lower frequency branch; (b), (e): intermediate branch; and (c), (f): upper branch. The dashed horizontal lines in (e) show the upper and lower limits for ϵ as $k \to 0$, see Fig. 3(c).

longitudinal components and the eccentricities are bounded by the associated values of $|q_k|$ and ϵ. In general, all modes have both longitudinal and transverse components. Note that in Fig. 4(e), the eccentricity is not defined for the plasmon at $\theta = 0$ as it is purely longitudinal. For $0 < \theta < \pi/2$, the eccentricity for $k \to 0$ is bounded from below and above by the $\theta \to 0$ and $\theta \to \pi/2$ limits shown in Fig. 3(c).

Partially different behavior is observed for $\beta = 0.5$, see Fig. 5. Since the frequencies of the lower branch are still bounded by those of the LS and LH modes, their properties are very similar to those in the case $\beta = 1.1$ [compare Figs. 4(a) and 5(a) and Figs. 4(d) and 5(d)]. In the intermediate branch, the upper frequency limit for $k_{\mathrm{crit}}a < 2.4$, where $\omega_{\mathrm{US}}(k_{\mathrm{crit}}) = \omega_{\mathrm{P}}(k_{\mathrm{crit}})$, is now the US mode, which is a purely transverse wave. This is reflected in the longitudinal

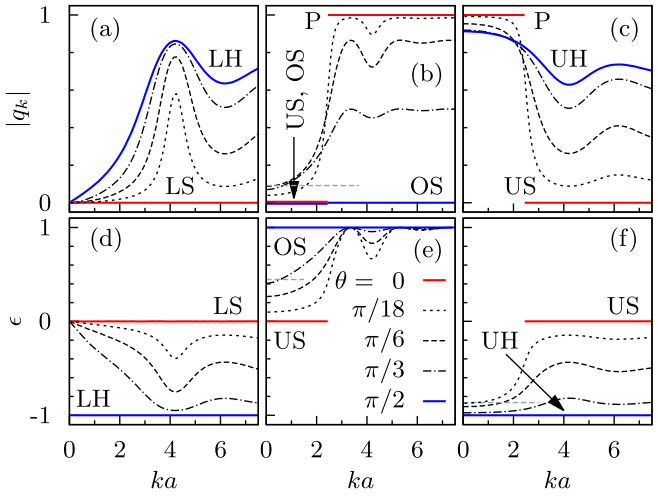

FIG. 5. Longitudinal component of the particle displacement, $|q_k|$, and modified eccentricity, ϵ, as a function of k and various angles for the same parameters as in Fig. 2(b) [$\Gamma = 100, \beta = 0.5$]—(a), (d): lower frequency branch; (b), (e): intermediate branch; and (c), (f): upper branch. The dashed horizontal lines show the respective upper limits as $k \to 0$: (b) $\theta \approx 0.67$, (e) $\theta \to \pi/2$, and (f) $\theta \to 0$, see Fig. 3. Note that in (b), both the US and OS modes have $|q_k| = 0$.

component of the wave, which is significantly smaller than for $\beta = 1.1$. As $k \to 0$, it has a maximum as a function of θ [indicated by the dashed line in Fig. 5(b)], see Fig. 3(a). In the upper branch, the mode now begins as a longitudinal wave at $\theta = 0$ and at small k (plasmon) compared to the transverse US mode in the case $\beta = 1.1$.

Different behavior is also observed for the eccentricity, as can be seen in Fig. 5(e). Compared to the case $\beta = 1.1$, the eccentricity of the intermediate branch now approaches 0 as $k \to 0$ and $\theta = 0$, corresponding to the US mode. In the upper branch, the eccentricity does not exceed a certain value $\epsilon_3(0)$ in the limit $k \to 0$, as shown in Figs. 5(f) and 3(d).

IV. CONCLUSIONS

To summarize, we have analyzed the wave spectrum of the strongly coupled magnetized OCP for arbitrary angles between the wave vector and the magnetic field. The crossover from parallel to perpendicular wave propagation depends on the magnetization $\beta = \omega_{\mathrm{c}}/\omega_{\mathrm{p}}$. In weak magnetic fields, $\beta < 1$, the frequencies of the principal modes parallel to the field intersect, and the transition behavior is largely dominated by avoided frequency crossings of the different wave modes, which is also reflected in their polarizations. In strong fields ($\beta > 1$), on the other hand, the modes are clearly separated. In this case, there is a critical angle at which the long-wavelength dispersion in the upper and lower branch changes sign. Since the collective modes determine the linear response behavior of the plasma, the results are important for a variety of transport processes such as diffusion,[9] or the plasma response to external fields.

It is important to compare the results of the QLCA with first-principle MD simulations, which, however, is beyond the scope of this paper. The mode spectrum presented here should be helpful for the interpretation of the simulations in the strong coupling limit. It would further be interesting to study the transition to moderately and weakly coupled systems, where the QLCA is not applicable. In particular, the plasmon dispersion in the unmagnetized OCP becomes positive for $\Gamma \lesssim 9.5 - 10$,[39] which is expected to have a strong effect on the mode crossings.

ACKNOWLEDGMENTS

We thank K. Golden for enlightening discussions and sharing his unpublished notes with us. This work was supported by the DFG via SFB TR24 (project A7), the DAAD via a postdoctoral fellowship (H.K.), and the RISE program (A.R.), and NSF grants PHY-0715227, PHY-1105005, and PHY-0813153.

APPENDIX: EIGENFREQUENCIES IN THE LIMIT $\theta \to \pi/2, ka \to 0$

Since the dispersion of the modes in the lower and intermediate branch changes from quadratic ($\theta \neq \pi/2$) to linear ($\theta \equiv \pi/2$) at small ka, the limit $\theta \to \pi/2$ will be inspected in more detail here. Similar to the expansion in ka for $\theta \neq \pi/2$ [Eq. (21)], we can derive an expansion in terms of $(\theta - \pi/2)$ for $ka \neq 0$. From Eq. (10), we get

$$\omega_1(k,\theta) \approx \omega_{\mathrm{LH}}(k)\left[1+\frac{\omega_{\mathrm{c}}^2(\omega_{\mathrm{OS}}^2-\omega_{\mathrm{P}}^2)\,(\theta-\pi/2)^2}{[\omega_{\mathrm{c}}^4+\omega_{\mathrm{c}}^2(2\omega_{\mathrm{OS}}^2+2\omega_{\mathrm{P}}^2-\Delta)+(\omega_{\mathrm{OS}}^2-\omega_{\mathrm{P}}^2)(\omega_{\mathrm{OS}}^2-\omega_{\mathrm{P}}^2+\Delta)]}\right], \tag{A1}$$

where

$$\Delta=\sqrt{(\omega_{\mathrm{P}}^2-\omega_{\mathrm{OS}}^2+\omega_{\mathrm{c}}^2)^2+4\omega_{\mathrm{c}}^2\omega_{\mathrm{OS}}^2}. \tag{A2}$$

In the long-wavelength limit, the term in brackets can be roughly approximated by

$$\begin{aligned}\omega_1(k,\theta) &\approx \omega_{\mathrm{LH}}(k)\left[1-\frac{(\theta-\pi/2)^2}{2k^2a^2}\right],\\ &\approx \omega_{\mathrm{p}}\frac{\sqrt{\alpha}\,ka}{\sqrt{1+\beta^2}}\left[1-\frac{(\theta-\pi/2)^2}{2\,k^2a^2}\right].\end{aligned} \tag{A3}$$

In addition, we used Eq. (16) in the second line for the LH mode.

An equivalent analysis can be carried out for the intermediate branch. For $ka \neq 0$, an expansion of Eq. (10) in $(\theta-\pi/2)$ leads to

$$\begin{aligned}\omega_2(k,\theta) &\approx \omega_{\mathrm{OS}}(k)\left[1+\left(\frac{\omega_{\mathrm{P}}^2}{\omega_{\mathrm{OS}}^2}-1\right)\frac{(\theta-\pi/2)^2}{2}\right]\\ &\approx \omega_{\mathrm{p}}\sqrt{\alpha}\,ka\left[1+\frac{(\theta-\pi/2)^2}{2\alpha\,k^2a^2}\right].\end{aligned} \tag{A4}$$

In the second line, we have expanded the term in brackets for small ka and used Eq. (15) for the OS mode, similar to Eq. (A3).

While the modes in the lower and intermediate branch are strictly quadratic in the long wavelength limit for $\theta \neq \pi/2$ [see Eqs. (20) and (21)], there exists a finite wavenumber interval where the dispersion is almost linear, and Eqs. (A3) and (A4) become approximately valid. This occurs in the close vicinity of $\theta \approx \pi/2$ and is illustrated in Fig. 6 for the lower branch. As θ approaches $\pi/2$, the range of validity for the quadratic dispersion becomes smaller, the linear behavior becomes apparent at finite ka and its range extends to increasingly lower ka, as suggested by the second term in Eq. (A3). For a similar discussion in the OCP crystal, see Ref. 24.

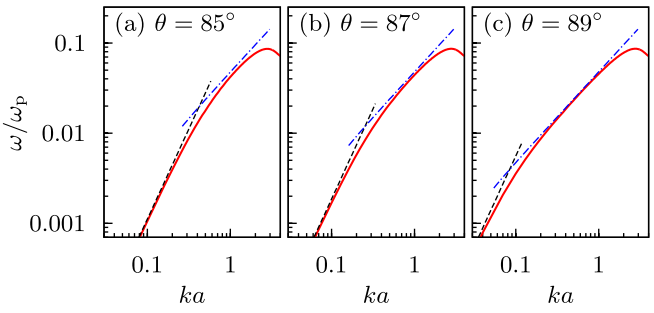

FIG. 6. Comparison of the numerical solution of Eq. (10) (solid lines) with the quadratic limit for $ka \to 0$ [Eq. (20), dashed lines], and Eq. (A3) for small but finite ka (dashed-dotted lines), which is shown for $3|\theta-\pi/2| < ka < 3$. The magnetization and coupling parameters are $\beta = 4$ and $\Gamma = 100$, respectively. We used $\alpha(\Gamma) \approx 0.0389$.[29,33]

[1]G. E. Morfill and A. V. Ivlev, Rev. Mod. Phys. **81**, 1353 (2009).
[2]M. Bonitz, C. Henning, and D. Block, Rep. Prog. Phys. **73**, 066501 (2010).
[3]A. V. Ivlev, H. Löwen, G. E. Morfill, and C. P. Royall, *Complex Plasmas and Colloidal Dispersions: Particle-Resolved Studies of Classical Liquids and Solids, Series in Soft Condensed Matter* (World Scientific, Singapore, 2012), Vol. 5.
[4]M. Schwabe, U. Konopka, P. Bandyopadhyay, and G. E. Morfill, Phys. Rev. Lett. **106**, 215004 (2011).
[5]J. Carstensen, F. Greiner, and A. Piel, Phys. Rev. Lett. **109**, 135001 (2012).
[6]S. Hamaguchi, R. T. Farouki, and D. H. E. Dubin, Phys. Rev. E **56**, 4671 (1997).
[7]Z. Donkó, G. J. Kalman, and K. I. Golden, Phys. Rev. Lett. **88**, 225001 (2002).
[8]M. Bonitz, Z. Donkó, T. Ott, H. Kählert, and P. Hartmann, Phys. Rev. Lett. **105**, 055002 (2010).
[9]T. Ott and M. Bonitz, Phys. Rev. Lett. **107**, 135003 (2011).
[10]F. Anderegg, D. H. E. Dubin, T. M. O'Neil, and C. F. Driscoll, Phys. Rev. Lett. **102**, 185001 (2009).
[11]A. Y. Potekhin, Phys. Usp. **53**, 1235 (2010).
[12]H. Kählert, J. Carstensen, M. Bonitz, H. Löwen, F. Greiner, and A. Piel, Phys. Rev. Lett. **109**, 155003 (2012).
[13]J. Carstensen, F. Greiner, L.-J. Hou, H. Maurer, and A. Piel, Phys. Plasmas **16**, 013702 (2009).
[14]M. Bonitz, H. Kählert, T. Ott, and H. Löwen, Plasma Sources Sci. Technol. **22**, 015007 (2013).
[15]G. Uchida, U. Konopka, and G. Morfill, Phys. Rev. Lett. **93**, 155002 (2004).
[16]B. Farokhi, M. Shahmansouri, and P. K. Shukla, Phys. Plasmas **16**, 063703 (2009).
[17]L.-J. Hou, P. K. Shukla, A. Piel, and Z. L. Mišković, Phys. Plasmas **16**, 073704 (2009).
[18]K. Jiang, Y.-H. Song, and Y.-N. Wang, Phys. Plasmas **14**, 103708 (2007).
[19]T. Ott, M. Bonitz, P. Hartmann, and Z. Donkó, Phys. Rev. E **83**, 046403 (2011).
[20]K. I. Golden, G. Kalman, and P. Wyns, Phys. Rev. B **48**, 8882 (1993).
[21]S. Ranganathan and R. E. Johnson, Phys. Rev. B **71**, 035339 (2005).
[22]T. Nagai and H. Fukuyama, J. Phys. Soc. Jpn. **51**, 3431 (1982).
[23]T. Nagai and H. Fukuyama, J. Phys. Soc. Jpn. **52**, 44 (1983).
[24]D. A. Baiko, Phys. Rev. E **80**, 046405 (2009).
[25]X.-F. Yang and Z.-X. Wang, Phys. Plasmas **19**, 073704 (2012).
[26]G. Kalman, K. I. Golden, and M. Minella, in *Strongly Coupled Plasma Physics*, edited by H. Van Horn and S. Ichimaru (University of Rochester Press, Rochester, 1994).
[27]T. Ott, H. Kählert, A. Reynolds, and M. Bonitz, Phys. Rev. Lett. **108**, 255002 (2012).
[28]I. M. Tkachenko, J. Ortner, and V. M. Rylyuk, Phys. Rev. E **57**, 4846 (1998).
[29]K. I. Golden, G. Kalman, and P. Wyns, Phys. Rev. A **46**, 3454 (1992); K. Golden, private communication (2012).
[30]G. Kalman and K. I. Golden, Phys. Rev. A **41**, 5516 (1990).
[31]K. I. Golden and G. J. Kalman, Phys. Plasmas **7**, 14 (2000).
[32]G. Kalman, M. Rosenberg, and H. E. DeWitt, Phys. Rev. Lett. **84**, 6030 (2000).
[33]G. S. Stringfellow, H. E. DeWitt, and W. L. Slattery, Phys. Rev. A **41**, 1105 (1990).
[34]M. S. Murillo, Phys. Rev. Lett. **85**, 2514 (2000).
[35]H. Ohta and S. Hamaguchi, Phys. Rev. Lett. **84**, 6026 (2000).
[36]This follows, e.g., from Vieta's formulas for the roots of a cubic equation (p. 17 in Ref. 40).
[37]J. Bittencourt, *Fundamentals of Plasma Physics* (Springer, New York, 2004).
[38]S. Ichimaru, *Basic Principles of Plasma Physics: A Statistical Approach* (Benjamin, MA, 1973).
[39]J. P. Mithen, J. Daligault, and G. Gregori, AIP Conf. Proc. **1421**, 68 (2012).
[40]*Handbook of Mathematical Functions With Formulas, Graphs, and Mathematical Tables*, edited by M. Abramowitz and I. A. Stegun (National Bureau of Standards, Washington, D.C., 10th printing, 1972).
[41]R. O. Genga, Int. J. Theor. Phys. **27**, 649 (1988).
[42]R. O. Genga, Int. J. Theor. Phys. **27**, 819 (1988).